Spin dynamics in the staircase kagome lattice compound $PbCu_3TeO_7$

Sungwon Yoon,[1,2,3] C. H. Lee,[1] S. Lee,[1] Y. S. Choi,[1] S.-H. Do,[1,4] M. Abdel-Jawad,[3] I. Watanabe,[3,*] B. J. Suh,[2,†] and Kwang-Yong Choi[1,‡]

[1]*Department of Physics, Chung-Ang University, Seoul 06974, Republic of Korea*

[2]*Department of Physics, The Catholic University of Korea, Bucheon 14662, Republic of Korea*

[3]*Meson Science Laboratory, RIKEN Nishina Center, 2-1, Hirosawa, Wako, Saitama 351-0198, Japan*

[4]*Max Planck POSTECH/Hsinchu Center for Complex Phase Materials, POSTECH, Pohang 37673, Republic of Korea*

(Received 22 August 2018; revised manuscript received 28 October 2018; published 3 December 2018)

Spin dynamics of the staircase kagome lattice $PbCu_3TeO_7$ was investigated by static magnetic susceptibility $\chi(T)$, high-field magnetization $M(H)$, and muon spin rotation/relaxation (μSR) measurements. $\chi(T)$ displays a sub-Curie power-law behavior $\chi(T) \sim T^{-\alpha}$ with changing exponent from $\alpha = 0.5$ to 0.3 crossing $T^* = 150$ K. We identify a spin-flop transition at $\mu_0 H = 8.5$ T and another field-induced anomaly at $\mu_0 H^* = 30$ T in $M(H)$. Our μSR results unveil that the magnetically inequivalent Cu(1) and Cu(2) spins develop site-specific magnetic structures through the successive magnetic transitions at $T_{N1} = 36$ K, $T_{N2} = 25$ K, and $T_{N3} = 17$ K. The magnetic anomalies of $PbCu_3TeO_7$ suggest that the Cu(1) and Cu(2) subsystems feature a largely distinct magnetism due to the presence of a dozen competing exchange interactions having largely different energy scales and thus the magnetism of $PbCu_3TeO_7$ is far more complex than the staircase kagome lattice.

DOI: 10.1103/PhysRevB.98.214401

I. INTRODUCTION

Two-dimensional (2D) $S = 1/2$ kagome antiferromagnets represent a fascinating physical model that harbors a quantum spin liquid featuring low-lying excitations with fractional quantum numbers [1–3]. The herbertsmithite $Cu_3Zn(OH)_6Cl_2$ and its polymorph kapellasite are the best material realization of an isotropic kagome lattice known to date [4,5]. In these materials, there is compelling evidence for the presence of quantum spin liquid, although some controversy on its precise flavor remains.

Quite often, however, real materials are plagued by a symmetry reduction from the ideal kagome structure, giving rise to spatially anisotropic exchange, longer range exchange, Dzyaloshinskii-Moriya and interlayer interactions. In most cases, lattice imperfections and the resultant perturbation terms are detrimental to quantum spin liquids. On the other hand, their interplay with geometric frustration can create a panoply of competing ground states with complex magnetic structures at zero magnetic field and field-induced topological magnetic excitations that lead to the observation of thermal Hall conductivity [6–10]. The prominent examples of anisotropic kagome systems include vesignieite $BaCu_3V_2O_8(OH)_2$, volborthite $Cu_3V_2O_7(OH)_2 \cdot 2H_2O$, $Rb_2Cu_3SnF_{12}$, and $PbCu_3TeO_7$ [11–15]. The vesignieite and volborthite are located in the magnetically ordered side, while $Rb_2Cu_3SnF_{12}$ stabilizes a pinwheel valence bond solid with a spin gap of 20 K.

The newly discovered $PbCu_3TeO_7$ has been proposed to form a distorted staircase kagome lattice [15–18]. $PbCu_3TeO_7$ contains two crystallographically different Cu sites, namely, the $Cu(1)O_6$ octahedra and $Cu(2)O_4$ tetrahedra [see Fig. 1(a)]. The underlying spin network resembles that of the prototypical staircase kagome compound $A_3V_2O_8$ (A = β-Cu,Ni,Co), which hosts two distinct incommensurate and two commensurate antiferromagnetic phases [19–21]. It is thus natural to expect that various temperature and energy scales involved in magnetic ordering processes of $PbCu_3TeO_7$ bring about many-faceted symmetry broken states.

The magnetic Cu^{2+} ($S = 1/2$) ions of $PbCu_3TeO_7$ (*Pnma* space group) are coupled through complex Cu(1,2)-O-Cu(1,2) superexchange paths to form a quasi-2D arrangement of buckled kagome layers in the *bc* planes. As sketched in Fig. 1(b), the different Cu-Cu bond lengths and the Cu-O-Cu bond angles yield four different nearest-neighbor (nn) exchange constants J_i (i = 1–4). In addition, electronic structure calculations unveil substantial second- and third-nn exchange interactions J_i (i = 5–8) as well as a number of interkagome exchange interactions mediated by Te atoms [not indicated in Fig. 1(b)] [15]. The substantial interlayer coupling is confirmed by the large hyperfine coupling constant of ^{125}Te [17]. Taken together, $PbCu_3TeO_7$ provides a playground to explore a crossover from a 2D staircase kagome to a three-dimensional frustrated magnetism with strong quantum fluctuations.

From the Curie-Weiss fitting to the high-T magnetic susceptibility $\chi(T)$, a Curie-Weiss temperature was evaluated to be $\Theta_{CW} = -150$ K [15]. Upon cooling, $PbCu_3TeO_7$ undergoes the successive magnetic transitions at $T_{N1} = 36$ K, $T_{N2} = 25$ K, and $T_{N3} = 17$ K. The sizable value of the frustration index $f = \Theta_{CW}/T_{N1} = 4.2$ points towards the presence of moderate spin frustration. It is noteworthy that the magnetic

*nabedon@riken.jp
†bjsuh@catholic.ac.kr
‡kchoi@cau.ac.kr

 ©2018 American Physical Society

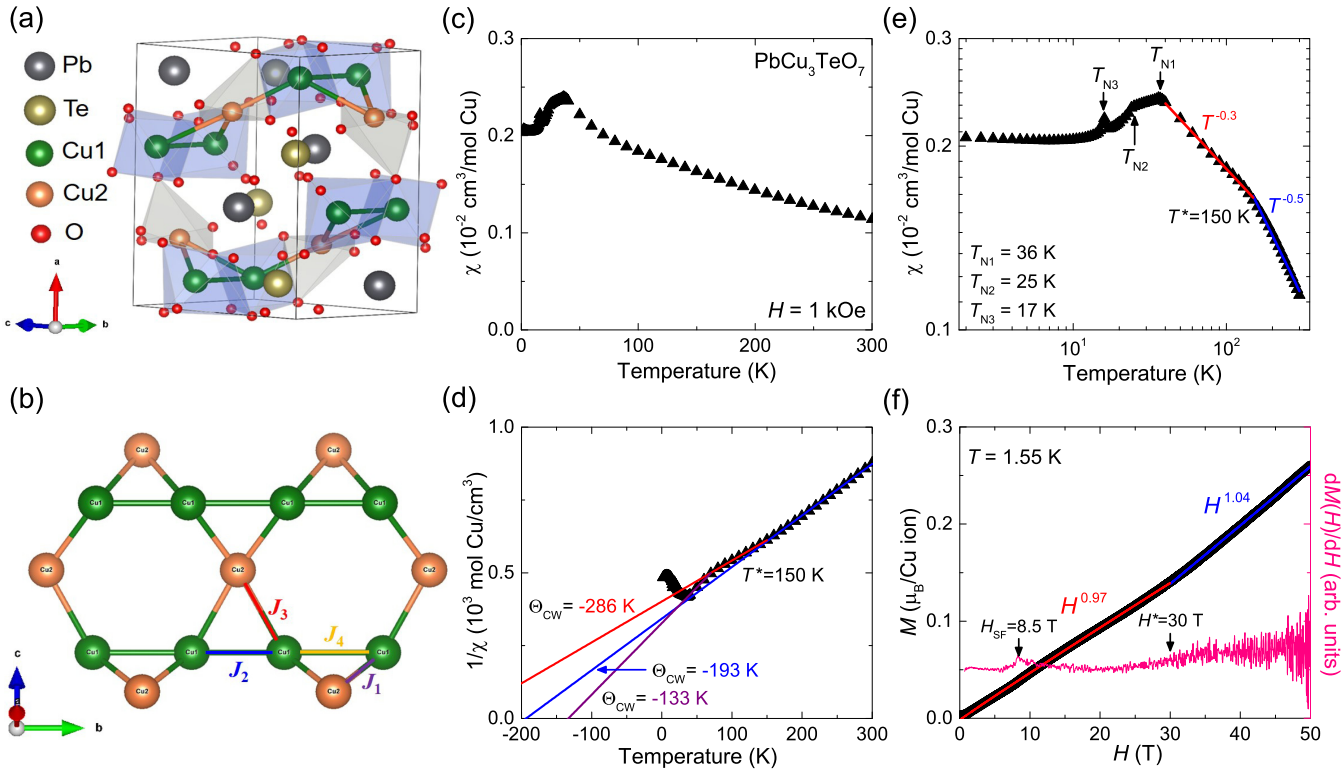

FIG. 1. (a) Crystal structure of $PbCu_3TeO_7$. Corner-shared triangles are formed by the Cu(1)O_6 octahedra and Cu(2)O_4 tetrahedra. The gray, gold, green, orange, and red spheres denote Pb, Te, Cu(1), Cu(2), and O ions, respectively. (b) A staircase kagome layer composed of four nearest-neighbor intrakagome couplings $J_i (i = 1–4)$. (c) Magnetic susceptibility of a polycrystalline $PbCu_3TeO_7$ sample as a function of temperature. (d) Temperature dependence of the inverse magnetic susceptibility. The solid lines are fits of the data to the Curie-Weiss law in the three different temperature ranges. (e) Log-log plot of the magnetic susceptibility vs temperature. The data are fitted to the power-law dependence $\chi(T) \sim T^{-\alpha}$. The vertical arrows indicate the magnetic anomalies. (f) High-field magnetization curve $M(H)$ measured at $T = 1.55$ K. The right y axis plots the field derivative of $M(H)/dH$. The vertical arrows are the spin-flop transition at $\mu_0 H_{SF} = 8.5$ T and the field-induced anomaly at $\mu_0 H^* = 30$ T.

transitions rely on a magnetic field direction and employed measurement techniques. For instance, the first-order magnetic transition at T_{N3} is hidden in the specific heat. On the other hand, the magnetic anomalies at T_{N1} and T_{N3} are apparent for $\mu_0 H \parallel a$, while the anomaly at T_{N2} becomes discernible only for $\mu_0 H \parallel c$ [15,18]. To clarify an origin of the field-direction dependence of the magnetic transitions, we employ a muon spin rotation/relaxation (μSR) technique, allowing for investigating internal static fields without applying an external magnetic field.

In this paper, we present a combined study of high-field magnetization and μSR towards understanding the nature of multiple magnetic transitions and associated spin dynamics of $PbCu_3TeO_7$. The salient findings are that $PbCu_3TeO_7$ develops site-specific magnetism at the magnetically inequivalent Cu(1) and Cu(2) sites. Our measurements suggest that the magnetic behavior of $PbCu_3TeO_7$ is more rich and complex than the purported staircase kagome lattice due to the presence of a dozen competing exchange interactions whose strengths vary over an order of magnitude.

II. EXPERIMENTAL DETAILS

Polycrystalline samples of $PbCu_3TeO_7$ were synthesized by the solid-state reaction method using a stoichiometric mixture of PbO (99.9% pure), TeO_2 (99.99%), and CuO (99.99%) chemicals in the high-pressure oxygen flow environments, following the similar recipe described in Ref. [15]. We checked the phase purity and crystal structure of the synthesized samples using the x-ray diffraction (XRD) method with Cu K_α radiation. Rietveld refinements of the XRD pattern revealed that the structural parameters of our samples agree nicely with the previously reported values [16].

DC magnetic susceptibility and isothermal-magnetization measurements were carried out using a superconducting quantum interference device (SQUID) magnetometer (Quantum Design MPMS-XL7). The magnetic susceptibilities were recorded over the temperature range of 2–300 K at an applied magnetic field of $H = 1$ kOe, and the isothermal magnetization curves were measured up to 7 T at $T = 2$ K and were used to calibrate the pulsed-field magnetization data. High-field magnetization measurements were conducted at the Dresden High Magnetic Field Laboratory using a nondestructive pulsed magnet that generates pulsed magnetic fields up to 60 T with the 25 ms duration. The magnetic moment was probed using an induction method with a pickup coil device at $T = 1.55$ K.

μSR experiments were performed on the CHRONUS spectrometer at the RIKEN-RAL Muon facility (Rutherford Appleton Laboratory, UK) as well as on the LAMPF

spectrometer at the M20 beamline in TRIUMF (Vancouver, Canada). We note that the pulsed muon beam utilized at the RIKEN-RAL Muon facility has its intrinsic limitation to temporal resolution in the initial time window of 0.1 μs due to the pulse width (FWHM) of 70 ns and the additional time required for storing the number of detected positrons. In contrast, continuous muon sources in TRIUMF have no time structure. The physical quantity measured with μSR is the time evolution of the muon spin polarization which reflects local magnetic fields of the target material. All of the time-differential muon spin polarization were analyzed by WiMDA [22].

III. RESULTS AND DISCUSSION

A. Static magnetic susceptibility and high-field magnetization

Figure 1(c) presents the temperature dependence of the static magnetic susceptibility $\chi(T)$ of the polycrystalline $PbCu_3TeO_7$ sample measured at $H = 1$ kOe. With decreasing temperature, $\chi(T)$ increases gradually and then forms a sharp maximum followed by kinks between 17 K and 36 K and finally levels off below 10 K. The kink and cusp features are associated with the magnetic anomalies at $T_{N1} = 36$ K, $T_{N2} = 25$ K, and $T_{N3} = 17$ K, reported in the prior work [see also Fig. 1(e)] [15]. Shown in Fig. 1(d) is the inverse susceptibility $1/\chi(T)$, which displays a linear T dependence only in limited temperature intervals.

Applying a Curie-Weiss fit to the $1/\chi(T)$ data yields the Curie-Weiss temperature $\Theta_{CW} = -193$ K and the effective magnetic moments $\mu_{eff} = 2.13\ \mu_B$ for temperatures above $T^* = 150$ K, $\Theta_{CW} = -286$ K, and $\mu_{eff} = 2.39\ \mu_B$ in the temperature range $T = 70$–150 K, and $\Theta_{CW} = -133$ K and $\mu_{eff} = 1.81\ \mu_B$ in the temperature range $T = 40$–70 K. Overall, the negative values of Θ_{CW} in the three distinct Curie-Weiss regimes suggest that the antiferromagnetic correlations are predominant over the nearly whole measured temperature range. The peculiar observation is a nonmonotonic change of Θ_{CW} as a function of temperature. One possible explanation is that the competing exchange interactions have opposite signs and largely different values of couplings. In addition, the effective magnetic moments obtained from the Curie-Weiss law are significantly enhanced than the spin-only value of 1.7 μ_B per Cu^{2+} ion. However, this may not be ascribed to the unquenched orbital magnetic moment because μ_{eff} was not extracted in a pure paramagnetic state (see below). High-temperature measurements above 300 K are indispensable for clarifying this point.

To articulate a non-Curie behavior, $\chi(T)$ is plotted on the log-log scale in Fig. 1(e). It is remarkable that $\chi(T)$ is described by a power-law increase $\chi(T) \sim T^{-\alpha}$ with $\alpha = 0.5$ for temperatures above $T^* = 150$ K. In the intermediate-T range of $T = 40$–150 K, the exponent is reduced to $\alpha = 0.3$. Such a sub-Curie law in the paramagnetic state is a hallmark of random magnetism [23–25]. We note that within the random magnetism scenario, the exponent is associated with a distribution of coupling constants. However, there is no apparent hint of chemical disorders in the studied system. Rather, a dozen competitive exchange couplings and frustrated geometry may be responsible for the emergent sub-Curie power-law behavior of the high-T magnetic susceptibility. As the exchange interactions differ by orders of magnitude in their strength, the magnetic correlations vary with a site and temperature. For instance, when the exchange interaction J_i is smaller than the thermal energy k_BT, the J_i exchange interaction is no longer active above T. With decreasing temperature, a growing number of the exchange interactions are switched on. This results in the variation of an effective spin network (or a degree of spin frustration) with temperature. In this manner, spin correlations acquire a spatiothermal dependence, leading to the net randomness. In this light, the crossover temperature T^* may reflect the change of an effective energy scale involving the effective exchange interactions.

Figure 1(f) shows the high-field magnetization curve $M(H)$ of $PbCu_3TeO_7$ measured at $T = 1.55$ K with pulsed magnetic fields up to 50 T. With increasing H, $M(H)$ increases almost linearly up to 30 T with a tiny kink at 8.5 T and then shows a steeper increase above $\mu_0H^* = 30$ T. In search for the field-induced transitions, we take the field derivative dM/dH. We can identify a small peak at $\mu_0H_{SF} = 8.5$ T in dM/dH and its associated small step in $M(H)$. Here, the small step is ascribed to a spin floplike transition expected for antiferromagnets. The slope change at $\mu_0H^* = 30$ T points to another field-induced anomaly. We recall that the downward concave magnetization is often observed in frustrated antiferromagnets whose pronounced quantum fluctuations or anisotropic exchange interactions lead to a suppression of magnetization. The distorted spin topology along with the complex exchange interactions of largely varying magnitude, however, renders it hard to identify its origin. The very recent single-crystal $M(H)$ data unveil that the field-induced phases rely on the applied field orientation [18], signifying an energy hierarchy and spatial anisotropy of involved exchange interactions.

B. ZF- and LF-μSR

With a view to elucidating the temperature evolution of local magnetic fields through the successive magnetic transitions, we performed μSR experiments, allowing probing the muon spin polarization as a function of time. Figure 2(a) exhibits the representative ZF-μSR spectra taken at the RIKEN-RAL Facility. In the paramagnetic phase ($T > 36$ K), the ZF-μSR spectrum features both a Gaussian damping and a slow muon spin relaxation at long times. This implies the presence of rapidly fluctuating dynamical fields arising from Cu moments. The RIKEN-RAL data at zero field were well described with the resulting relaxation function,

$$A(t) = A_{bg} + A_1e^{-\lambda t} + A_2e^{-(\sigma t)^2}, \quad (1)$$

where A_i is the relative amplitude of the two different components and λ and σ are the relaxation rates. The temperature-independent A_{bg} originates from a muon spin relaxation from muons implanted in the silver sample holder or the cryostat.

As the temperature is lowered below T_{N1}, the initial asymmetry drops rapidly while developing muon spin oscillation. The oscillatory signal confirms the occurrence of long-range magnetic order, in agreement with the above magnetic susceptibility data. Noticeably, the long-time muon

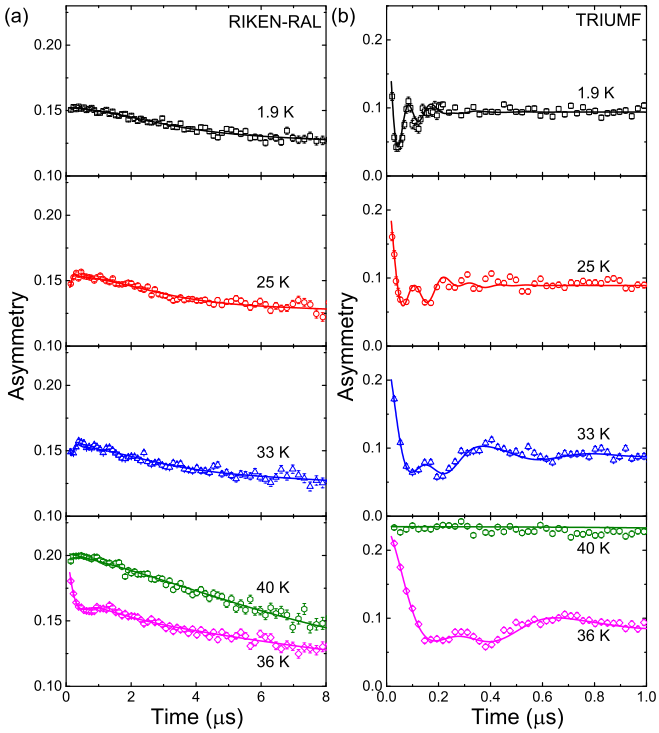

FIG. 2. (a) Representative time-differential ZF-μSR spectra taken at RIKEN-RAL for $PbCu_3TeO_7$ at selected temperatures. (b) Temperature dependence of ZF-μSR spectra recorded at TRIUMF in a temperature range $T = 1.9$–40 K. The solid lines represent fits to the data as described in the text.

polarization is subject to a substantial exponential relaxation. This demonstrates the persistence of strongly fluctuating magnetic moments into the ordered state. In the AFMI phase (25 K $< T <$ 36 K), the ZF-μSR spectra are modeled with the following relaxation function,

$$A(t) = A_{\rm bg} + A_1 e^{-\lambda t} + A_2 e^{-\Lambda t} \cos(2\pi f t + \phi), \quad (2)$$

where f is the muon Larmor frequency and ϕ is the initial phase of the oscillatory signal.

For temperatures below $T_{\rm N2}$, however, a faster muon precession becomes no longer resolvable due to a poor time resolution of the pulse muon beam. Rather, the RIKEN-RAL data in the AFMII (17 K $< T <$ 25 K) and AFMIII ($T <$ 17 K) phases are captured by Eq. (1), preventing from systematically tracing the temperature evolution of internal magnetic fields through the phase transitions. This motivates us to further employ a continuous muon source.

Figure 2(b) presents the early-time ZF-μSR spectra recorded with the LAMPF spectrometer at TRIUMF. Below 36 K, the CW-μSR spectra reveal clearly two oscillating components, which were not resolved with the pulse muon beam. The two distinct frequencies mean the presence of magnetically inequivalent muon sites in the material. In the three magnetic phases, the TRIUMF data were modeled with the same relaxation function,

$$A(t) = A_{\rm bg} + A_0 e^{-(\sigma t)^2} + \sum_{i=1}^{2} A_i e^{-\Lambda_i t} \cos(2\pi f_i t + \phi_i). \quad (3)$$

Here, A_0 and A_i are for the relative amplitudes of the relaxing and oscillating components, respectively.

Several comments are in order concerning the relaxation function in the magnetically ordered phase. First, there is no evidence for changes in the form of the asymmetry line shape through the three different phases. More specifically, the simple sinusoidal oscillation is sufficient to describe all of the ordered data with no use of zeroth-order Bessel functions $J_0(2\pi f t)$, which is appropriate for incommensurate magnetic order. This suggests that a distribution of the magnitudes of the static local magnetic fields shows little variation with the phase transitions. This is in sharp contrast to the staircase kagome compound $Ni_3V_2O_8$, in which an obvious change of the μSR relaxation form is induced by the commensurate-to-incommensurate transition [26]. Second, a successful fit of the measured spectra calls for the inclusion of a Gaussian relaxation function. This is reminiscent of the so-called undecouplable Gaussian relaxation reported in a range of kagome related systems including $SrCr_8Ga_4O_{19}$ and its relatives $Ni_3V_2O_8$, $ZnCu_3(OH)_6Cl_2$, and $YBaCo_4O_7$ [26–31]. However, it is far from unclear whether $PbCu_3TeO_7$ and the above-mentioned kagome related compounds share the same origin of the Gaussian relaxation. Noteworthy is that quenched disorders were inferred from a second zero-field NMR signal in the previous NMR measurements [17]. The presence of the quenched disorders in the background of spatiothermally random magnetic correlations may account for the Gaussian relaxation component in Eq. (3).

We next turn to the fitting results. Figure 3 summarizes the T dependences of the fitting parameters. The frequency of the oscillations is given by $f_i = \gamma_\mu B_i/2\pi$. Here $\gamma_\mu = 2\pi \times 135.5$ MHz/T is the muon gyromagnetic ratio and B_i is the local field at the muon site. On cooling down below $T_{\rm N}$, $f_i(T)$ displays an order-parameter-like increase. The fit of $f_i(T)$ to a phenomenological function $f_i(T) = f_i(0)[1 - (T/T_{\rm N})]^\beta$ with $\beta = 0.38$ (0.34) for $i = 1$ (2) reveals a distinct anomaly. $f_1(T)$ (the pink circles) is largely described by the single function over the three phases. In contrast, $f_2(T)$ (the green squares) undergoes a steplike decrease at $T_{\rm N2}$, indicative of a tiny reorientation of the spins. In addition, the relaxation rates also show a drastic, disparate change at $T_{\rm N2}$. As $T \to T_{\rm N2}$, $\Lambda_1(T)$ drops toward zero, whereas $\Lambda_2(T)$ exhibits a sharp increase and then levels off. The muon-site dependent $f_i(T)$ and $\Lambda_i(T)$ through $T_{\rm N2}$ imply that the two magnetically inequivalent muon sites behave disparately across the AFMI-to-AFMII transition. On entering the AFMII phase, the steplike increase of $\Lambda_2(T)$ points towards the enhanced magnetic fluctuations, whereas the sharp drop of $\Lambda_1(T)$ to zero means the frozen magnetic moments in the MHz μSR time window. The temperature evolution of the relative amplitudes is parallel to that of $f_i(T)$. The drastic changes in relaxation rates are evidence to a phase transition, and those might be as a result of critical fluctuations in the order parameter.

We recall that the similar site-specific anomalies of the μSR parameters were observed in the anisotropic spin tetramer system $CdCu_2(BO_3)_2$ with four inequivalent exchange couplings [32]. Similarly to $PbCu_3TeO_7$, $CdCu_2(BO_3)_2$ consisting of the Cu(1)O_6 octahedra and Cu(2)O_4 tetrahedra shows two muon-spin precessions in the

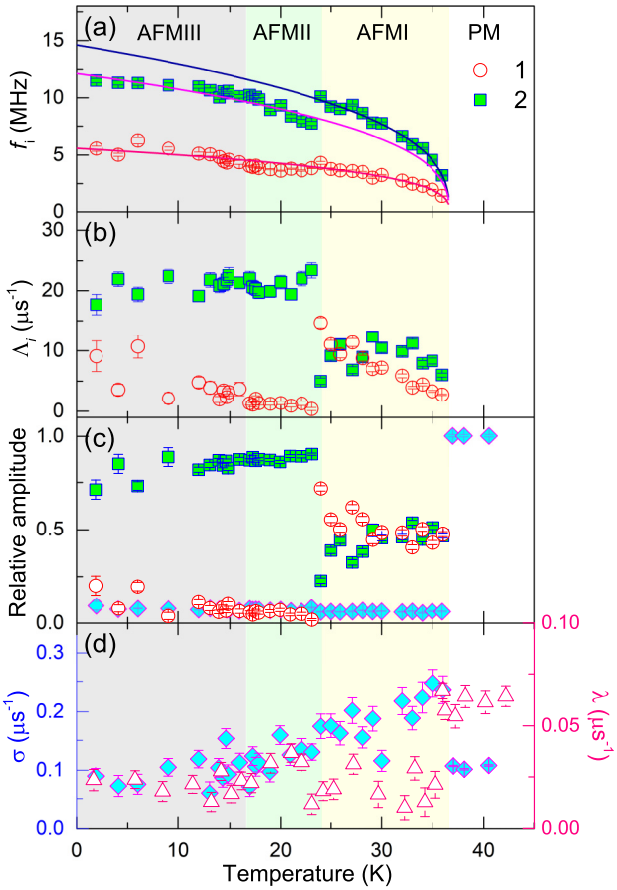

FIG. 3. (a) Temperature dependence of the muon-spin-precession frequencies f_i. The solid lines are fits to the phenomenological expression $[1-(T/T_N)]^\beta$, and the dashed line is a guide to the eye. (b) Temperature dependence of the depolarization rates Λ_i. (c) Normalized relative volume fractions as a function of temperature. (d) Temperature dependence of the longitudinal relaxation rates σ (diamond symbols obtained from the TRIUMF data) and λ (open triangle symbols obtained from the RIKEN-RAL data). The shaded regions are the three different magnetic phases.

long-range ordered state. Considering that the muons normally reside near an apical oxygen of each Cu(1) and Cu(2) sites as well as in comparison to the neutron diffraction results, the two frequencies were assigned to local dipolar fields arising from the two magnetically different Cu(1) and Cu(2) sites. The same reasoning may apply to the studied compound. Under this assumption, we reach a conclusion that the AFMI-to-AFMII transition involves the reordering of one of the Cu spins while the other Cu spin is hardly affected. The site-specific spin reordering toward the c axis may explain why the T_{N2} anomaly is visible only for $\mu_0 H \parallel c$ [15,18]. A neutron diffraction study is requested to ascertain this scenario.

Unlike the AFMI-to-AFMII transition, no appreciable change of the μSR parameters is observed across the AFMII-to-AFMIII phase transition. The internal field, relaxation rates, and relative amplitudes exhibit little change through T_{N3}. This means that no substantial entropy is involved through this first-order transition, most probably driven by

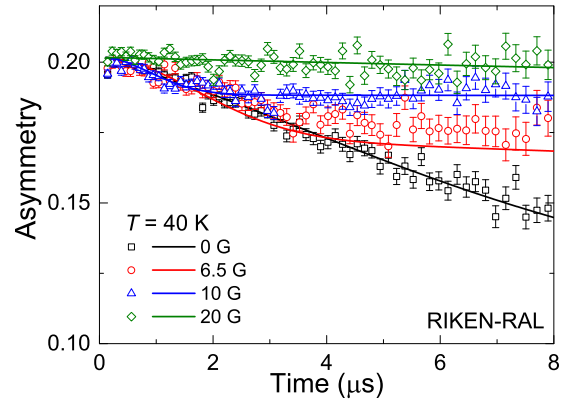

FIG. 4. Longitudinal-field dependence of μSR spectra measured at $T = 40$ K in a magnetic field $H = 0$–20 G.

magnetoelastic coupling. In Fig. 3(d), we compare the T dependence of the longitudinal relaxation rates σ and λ determined by the TRIUMF and RIKEN-RAL data, respectively. $\sigma(T)$ shows a critical behavior only at T_{N1}. $\lambda(T)$ display a sharp change at both the second-order phase transitions T_{N1} and T_{N2}, while showing no noticeable anomalies at the first-order phase transition T_{N3}.

We next turn to the longitudinal-field (LF) dependence of the μSR spectra measured at $T = 40$ K shown in Fig. 4. The data were taken at the RIKEN-RAL facility. Applying a 20 G field parallel to the initial muon polarization leads to a nearly full polarization of the LF-μSR spectra due to a spin-locking effect. Similarly to $PbCu_3TeO_7$, the LF-μSR spectra of $La_{2-x}Sr_xCuO_4$ ($x = 0.115$) showed an almost full polarization in LF of 20 G [33]. This is interpreted in terms of nullification of both static and dynamic internal fields at the muon site by the application of a weak LF. The similar thing may happen to $PbCu_3TeO_7$, which is characterized by the largely different magnetism between the Cu(1) and Cu(2) subsystems.

To analyze a field dependence of the longitudinal relaxation rate, we applied the Redfield formula (not shown in here). Fitting yields a fluctuation frequency $\nu = 0.20$ MHz. This value turns out to be much smaller than $\nu = 150$ MHz of $ZnCu_3(OH)_6Cl_2$ known for the putative spin-liquid state [30]. The reduced ν in our compound indicates that the spins are in a slowing-down regime rather than in a fast fluctuating limit. Strictly speaking, the Redfield formula is valid only in the fast fluctuation limit. Thus, the extracted $\nu = 0.20$ MHz in $PbCu_3TeO_7$ should be taken as an indication that its magnetism is far from quantum spin liquids.

IV. CONCLUSIONS

μSR combined with static magnetic susceptibility and magnetization measurements allows us to probe the temperature evolution of the local field distribution in the three different phases. At first glance, the multiple transitions of $PbCu_3TeO_7$ are reminiscent of a class of staircase kagome materials. Our detailed study unravels that the purported staircase kagome model is not sufficient to capture all landscapes of magnetic behaviors. In addition to the frustrated spin topology, an energy hierarchy of the two magnetically inequivalent

Cu(1) and Cu(2) spins should be further invoked due to the presence of a dozen competing exchange interactions whose strengths range over an order of magnitude.

First, the high-field magnetization shows a downward concave curvature, indicative of the suppressed magnetization due to frustration-induced quantum fluctuations or anisotropic magnetic interactions. We further identify a spin floplike transition at $\mu_0 H_{SF} = 8.5$ T and the second field-induced anomaly at $\mu_0 H^* = 30$ T. Second, $\chi(T)$ shows the sub-Curie power-law dependence $\chi(T) \sim T^{-\alpha}$, while changing the exponent from $\alpha = 0.5$ to 0.3 on cooling down through $T^* = 150$ K. Such a sub-Curie behavior is indicative of the presence of random interactions. Since there are no obvious chemical disorders in $PbCu_3TeO_7$, a spatiothermal randomness in magnetic correlations is proposed. We call for a further theoretical study to clarify whether a dozen exchange interactions with energy hierarchy and frustrated geometry can induce random magnetism. In the random magnet scenario, the crossover temperature T^* marks a switching of an effective energy scale of involved exchange interactions. Third, the ZF-μSR results reveal a site-specific evolution of the magnetic structure in each transition, while showing no drastic change of local internal magnetic fields. The second transition at $T_{N2} = 25$ K involves the spin reordering of one Cu subsystem. The third transition at $T_{N3} = 17$ K is hardly seen by μSR.

The subtle, site-specific development of the magnetic structure suggests that the Cu(1) and Cu(2) subsystems, on one hand, are largely discriminated in their effective energy scale and their ordering pattern and, on the other hand, are tuned by a competition of longer-range and interkagome layer interactions. This partly explains the phenomena that the magnetic transitions are dependent on the field orientations. Due to the presence of a dozen competing exchange interactions with a large distribution of their strengths, the magnetism of $PbCu_3TeO_7$ goes beyond the simple staircase kagome model.

ACKNOWLEDGMENTS

We would like to thank B. Hitti for his assistance with the μSR experiments at TRIUMF. S.Y. was supported by RIKEN International Program Associate (IPA) Program. C.H.L. was supported by the Chung-Ang University Excellent Student Scholarship.

[1] G. Misguich and C. Lhuillier, in *Frustrated Spin Systems*, edited by H. T. Diep (World Scientific, Singapore, 2005).
[2] M. R. Norman, Rev. Mod. Phys. **88**, 041002 (2016).
[3] H. J. Liao, Z. Y. Xie, J. Chen, Z. Y. Liu, H. D. Xie, R. Z. Huang, B. Normand, and T. Xiang, Phys. Rev. Lett. **118**, 137202 (2017), and references therein.
[4] T.-H. Han, J. S. Helton, S. Chu, D. G. Nocera, J. A. Rodriguez-Rivera, C. Broholm, and Y. S. Lee, Nature (London) **492**, 406 (2012).
[5] B. Fåk, E. Kermarrec, L. Messio, B. Bernu, C. Lhuillier, F. Bert, P. Mendels, B. Koteswararao, F. Bouquet, J. Ollivier, A. D. Hillier, A. Amato, R. H. Colman, and A. S. Wills, Phys. Rev. Lett. **109**, 037208 (2012).
[6] A. B. Harris, C. Kallin, and A. J. Berlinsky, Phys. Rev. B **45**, 2899 (1992).
[7] J.-C. Domenge, P. Sindzingre, C. Lhuillier, and L. Pierre, Phys. Rev. B **72**, 024433 (2005).
[8] V. A. Zyuzin and G. A. Fiete, Phys. Rev. B **85**, 104417 (2012).
[9] P. H. Y. Li, R. F. Bishop, C. E. Campbell, D. J. J. Farnell, O. Götze, and J. Richter, Phys. Rev. B **86**, 214403 (2012).
[10] S. A. Owerre, Europhys. Lett. **117**, 37006 (2017).
[11] M. A. Lafontaine, A. L. Bail, and G. Férey, J. Solid State Chem. **85**, 220 (1990).
[12] Y. Okamoto, H. Yoshida, and Z. Hiroi, J. Phys. Soc. Jpn. **78**, 033701 (2009).
[13] K. Morita, M. Yano, T. Ono, H. Tanaka, K. Fujii, H. Uekusa, Y. Narumi, and K. Kindo, J. Phys. Soc. Jpn. **77**, 043707 (2008).
[14] K. Matan, T. Ono, Y. Fukumoto, T. J. Sato, J. Yamaura, M. Yano, K. Morita, and H. Tanaka, Nat. Phys. **6**, 865 (2010).
[15] B. Koteswararao, R. Kumar, Jayita Chakraborty, B.-G. Jeon, A. V. Mahajan, I. Dasgupta, K. H. Kim, and F. C. Chou, J. Phys.: Condens. Matter **25**, 336003 (2013).
[16] B. Wedel and H. Mueller-Buschbaum, Z. Naturforsch. B **51**, 1587 (1996).
[17] J. Dai, P.-S. Wang, S.-S. Sun, F. Pang, J.-S. Zhang, X.-L. Dong, G. Yue, K. Jin, J.-Z. Cong, Y. Sun, and W.-Q. Yu, Chin. Phys. Lett. **32**, 127503 (2015).
[18] K. Yoo, B. Koteswararao, J. Kang, A. Shahee, W. Nam, F. F. Balakirev, V. S. Zapf, N. Harrison, A. Guda, N. Ter-Oganessian, and K. H. Kim, npj Quantum Mater. **3**, 45 (2018).
[19] N. Rogado, G. Lawes, D. A. Huse, A. P. Ramirez, and R. J. Cava, Solid State Commun. **124**, 229 (2002).
[20] N. Rogado, M. K. Haas, G. Lawes, D. A. Huse, A. P. Ramirez, and R. J. Cava, J. Phys.: Condens. Matter **15**, 907 (2003).
[21] G. Lawes, M. Kenzelmann, N. Rogado, K. H. Kim, G. A. Jorge, R. J. Cava, A. Aharony, O. Entin-Wohlman, A. B. Harris, T. Yildirim, Q. Z. Huang, S. Park, C. Broholm, and A. P. Ramirez, Phys. Rev. Lett. **93**, 247201 (2004).
[22] F. L. Pratt, Physica B **289-290**, 710 (2000).
[23] S.-k. Ma, C. Dasgupta, and C.-k. Hu, Phys. Rev. Lett. **43**, 1434 (1979).
[24] J. E. Hirsch and J. V. Jose, Phys. Rev. B **22**, 5339 (1980).
[25] A. H. Castro Neto, G. Castilla, and B. A. Jones, Phys. Rev. Lett. **81**, 3531 (1998).
[26] T. Lancaster, S. J. Blundell, P. J. Baker, D. Prabhakaran, W. Hayes, and F. L. Pratt, Phys. Rev. B **75**, 064427 (2007).
[27] Y. J. Uemura, A. Keren, K. Kojima, L. P. Le, G. M. Luke, W. D. Wu, Y. Ajiro, T. Asano, Y. Kuriyama, M. Mekata, H. Kikuchi, and K. Kakurai, Phys. Rev. Lett. **73**, 3306 (1994).
[28] A. Keren, Y. J. Uemura, G. Luke, P. Mendels, M. Mekata, and T. Asano, Phys. Rev. Lett. **84**, 3450 (2000).
[29] D. Bono, P. Mendels, G. Collin, N. Blanchard, F. Bert, A. Amato, C. Baines, and A. D. Hillier, Phys. Rev. Lett. **93**, 187201 (2004).

[30] P. Mendels, F. Bert, M. A. de Vries, A. Olariu, A. Harrison, F. Duc, J. C. Trombe, J. S. Lord, A. Amato, and C. Baines, Phys. Rev. Lett. **98**, 077204 (2007).

[31] S. Lee, W. Lee, K. J. Lee, B. J. Kim, B. J. Suh, H. Zheng, J. F. Mitchell, and K.-Y. Choi, Phys. Rev. B **97**, 104409 (2018).

[32] W.-J. Lee, S.-H. Do, Sungwon Yoon, Z. H. Jang, B. J. Suh, J. H. Lee, A. P. Reyes, P. L. Kuhns, H. Luetkens, and K.-Y. Choi, Phys. Rev. B **90**, 214416 (2014).

[33] I. Watanabe, T. Adachi, S. Yairi, Y. Koike, and K. Nagamine J. Phys. Soc. Jpn. **77**, 124716 (2008).